New Cross-Sections for ^{nat}Mo(α,x) Reactions and Medical ^{97}Ru Production Estimations with Radionuclide Yield Calculator

Mateusz Sitarz [1,2,3,*], **Etienne Nigron** [4], **Arnaud Guertin** [4], **Férid Haddad** [1,4] **and Tomasz Matulewicz** [2]

[1]   Groupement d'Intérêt Public ARRONAX, 44817 Saint-Herblain CEDEX, France; haddad@subatech.in2p3.fr
[2]   Faculty of Physics, University of Warsaw, 02-093 Warszawa, Poland; Tomasz.Matulewicz@fuw.edu.pl
[3]   Heavy Ion Laboratory, University of Warsaw, 02-093 Warszawa, Poland
[4]   Subatech, CNRS/IN2P3, IMT Atlantique, Université de Nantes, CS 20722 44307 Nantes CEDEX, France;
      nigron@subatech.in2p3.fr (E.N.); Arnaud.Guertin@subatech.in2p3.fr (A.G.)
*   Correspondence: mateusz.sitarz@univ-nantes.fr

Abstract: The production of ^{97}Ru, a potential Single Photon Emission Computed Tomography (SPECT) radioisotope, was studied at ARRONAX. The cross-section of ^{nat}Mo(α,x)^{97}Ru reaction was investigated in the range of 40–67 MeV irradiating the ^{nat}Mo and Al stacked-foils. The activities of ^{97}Ru and other radioactive contaminants were measured via gamma spectroscopy technique. A global good agreement is observed between obtained cross-section results, previously reported values and TENDL-2017 predictions. Additionally, Radionuclide Yield Calculator, a software that we made available for free, dedicated to quickly calculate yields and plan the irradiation for any radioisotope production, was introduced. The yield of investigated nuclear reactions indicated the feasibility of ^{97}Ru production for medical applications with the use of α beam and Mo targets opening the way to a theranostic approach with ^{97}Ru and ^{103}Ru.

Keywords: SPECT; cyclotron; medical radioisotope production; radioactive impurities; cross-section; stacked-foils; gamma spectroscopy; thick target yield; Radionuclide Yield Calculator

1. Introduction

The ^{97}Ru radioisotope was first acknowledged as medically interesting in 1970 [1] and is even studied in recent measurements [2,3]. It has a half-life of 2.9 d allowing non-local production and emits low-energy high-intensity gamma lines (see Table 1) which have favorable characteristics for prolonged Single Photon Emission Computed Tomography (SPECT) examinations. It decays only by electron capture (EC) which lowers the contribution to the dose as compared to β^+ decays. It has a theranostic matched pair in the form of ^{103}Ru ($T_{1/2}$ = 39.26 d) that decays to the short-lived Auger emitter ^{103m}Rh ($T_{1/2}$ = 56.12 min), a promising gamma-free therapeutic agent. Moreover, ruthenium element has a rich chemistry associated with its various oxidation states (II, III, IV and VIII) and forms more stable compounds compared to the SPECT-standard ^{99m}Tc [4]. Many radioactive Ru-labeled compounds have been studied and found applications as summarized recently by [5], in particular as the chemotherapy agents [6,7].

Due to these interesting characteristics, many studies on production of ^{97}Ru have been conducted. The reactor route via ^{96}Ru(n,γ)^{97}Ru was reported by [1] but it yields very low specific activity which may limit its use for some applications such as molecular imaging. To obtain high specific activity product, one can use charged projectile from accelerators. In case of cyclotron routes, the first and most used reaction is ^{103}Rh(p,spall)^{97}Ru with 200 MeV proton beam and natural rhodium target,

as suggested by [8]. While producing high amount of activity of no-carrier-added (NCA) ^{97}Ru, this method requires high energy protons but no details about the impurity levels were reported. Another reaction route is the ^{103}Rh(p,x)^{97}Ru reaction using 60 MeV proton beam [9]; the ^{97}Ru production yield is very high but accompanied by Tc radioactive impurities which are difficult to discard even after the chemical separation step. A very feasible option is the ^{99}Tc(p,3n)^{97}Ru reaction suggested by [10] and studied later up to 100 MeV by [4,11,12] as it produces significant amounts of ^{97}Ru with very small amount of radioactive impurities. However, the availability of ^{99}Tc radioactive target is an issue. Later, experimental excitation functions were reported for ^{nat}Ag(p,x)^{97}Ru up to 80 MeV by [13] and for ^{nat}Pd(p,x)^{97}Ru up to 70 MeV by [14]. These two production routes have much smaller cross-section, hence ^{97}Ru production would require long irradiation time and would contain a substantial amount of radioactive impurities. In case of deuteron beam, the available reaction ^{96}Ru(d,x)^{97}Ru studied by [15] is favorable but would produce low specific activity as the target material is an isotope of the nuclide of interest. Some groups have also investigated more exotic projectiles such as helium-3 through ^{nat}Mo(^{3}He,x)^{97}Ru [16], ^{93}Nb(^{7}Li,3n)^{97}Ru [17] and ^{89}Y(^{12}C,p3n)^{97}Ru [2,18]. In these cases, after chemical separation, low level of radioactive impurities can be achieved but the availability of these beams is scarce making these processes not suitable to launched clinical trials. Finally, the cross-sections for α-induced reactions on Mo were investigated by [19]. ^{nat}Mo(α,x)^{97}Ru production and impurities up to 40 MeV were thoroughly studied in [3,20].

In this work, we investigate the optimization of ^{nat}Mo(α,x)^{97}Ru production route and extend the available cross-section data to higher energy in coherence with commercially available cyclotrons, [21] which are able to deliver up to about 70 MeV alpha beam. We also report on the coproduction of the measured radioactive impurities (listed in Table 1) via ^{nat}Mo(α,x) and explore the possible commercial production of ^{97}Ru with the α beam on Mo target using the software Radionuclide Yield Calculator (RYC) that we developed and made freely available to the community.

Table 1. Nuclear data [22] of ^{97}Ru and observed radionuclidic contaminants as well as reactions contributing to their formation during the irradiation of ^{nat}Mo target*.

Radionuclide	$T_{1/2}$	Decay Mode (%)	γ-Lines [keV] and Intensities** (%)	Contributing Reactions***	Q-Value [MeV]
^{97}Ru	2.83 d	EC (100)	215.7 (85.8) 324.5 (10.8)	^{94}Mo(α,n)^{97}Ru	−7.9
				^{95}Mo(α,2n)^{97}Ru	−15.3
				^{96}Mo(α,3n)^{97}Ru	−24.5
				^{97}Mo(α,4n)^{97}Ru	−31.3
				^{98}Mo(α,5n)^{97}Ru	−41.6
				^{100}Mo(α,7n)^{97}Ru	−54.1
^{89g}Zr	78.4 h	β^{+} (23), EC (77)	908.96 (100)	^{92}Mo(α,x)^{89tot}Zr	−16.7
				^{94}Mo(α,x)^{89tot}Zr	−14.0
				^{95}Mo(α,x)^{89tot}Zr	−21.4
				^{96}Mo(α,x)^{89tot}Zr	−30.6
				^{97}Mo(α,x)^{89tot}Zr	−37.4
				^{98}Mo(α,x)^{89tot}Zr	−46.0
				^{100}Mo(α,x)^{89tot}Zr	−60.2
				^{92}Mo(α,x)^{89tot}Nb→^{89tot}Zr	−21.1
				^{94}Mo(α,x)^{89tot}Nb→^{89tot}Zr	−38.9
				^{95}Mo(α,x)^{89tot}Nb→^{89tot}Zr	−46.2
				^{96}Mo(α,x)^{89tot}Nb→^{89tot}Zr	−55.4
				^{97}Mo(α,x)^{89tot}Nb→^{89tot}Zr	−62.2
				^{98}Mo(α,x)^{89tot}Nb→^{89tot}Zr	−70.9
				^{100}Mo(α,x)^{89tot}Nb→^{89tot}Zr	−85.1

Table 1. *Cont.*

Radionuclide	$T_{1/2}$	Decay Mode (%)	γ-Lines [keV] and Intensities** (%)	Contributing Reactions***	Q-Value [MeV]
^{96g}Tc	4.28 d	EC (100)	778.22 (100) 812.58 (82) 849.93 (98) 1126.97 (15.2)	^{94}Mo(α,x)^{96tot}Tc	−13.3
				^{95}Mo(α,x)^{96tot}Tc	−14.4
				^{96}Mo(α,x)^{96tot}Tc	−23.7
				^{97}Mo(α,x)^{96tot}Tc	−30.4
				^{98}Mo(α,x)^{96tot}Tc	−39.0
				^{100}Mo(α,x)^{96tot}Tc	−53.3
^{99}Mo	65.9 h	β^- (100)	140.51 (89.43) 739.50 (12.13)	^{97}Mo(α,2p)^{99}Mo	−13.7
				^{98}Mo(α,x)^{99}Mo	−14.7
				^{100}Mo(α,x)^{99}Mo	−8.3
^{95g}Tc	20.0 h	EC (100)	765.8 (93.82)	^{92}Mo(α,n)^{95g}Tc	−5.7
				^{94}Mo(α,x)^{95g}Tc	−14.9
				^{95}Mo(α,x)^{95g}Tc	−22.3
				^{96}Mo(α,x)^{95g}Tc	−31.4
				^{97}Mo(α,x)^{95g}Tc	−38.3
				^{98}Mo(α,x)^{95g}Tc	−46.9
				^{100}Mo(α,x)^{95g}Tc	−61.1
				^{92}Mo(α,n)^{95}Ru$\rightarrow^{95g}$Tc	−9.0
				^{94}Mo(α,3n)^{95}Ru$\rightarrow^{95g}$Tc	−26.7
				^{95}Mo(α,4n)^{95}Ru$\rightarrow^{95g}$Tc	−34.1
				^{96}Mo(α,5n)^{95}Ru$\rightarrow^{95g}$Tc	−43.3
				^{97}Mo(α,6n)^{95}Ru$\rightarrow^{95g}$Tc	−50.1
				^{98}Mo(α,7n)^{95}Ru$\rightarrow^{95g}$Tc	−58.7
				^{100}Mo(α,9n)^{95}Ru$\rightarrow^{95g}$Tc	−73.0

* ^{nat}Mo composition: ^{92}Mo (14.6%), ^{94}Mo (9.2%), ^{95}Mo (15.9%), ^{96}Mo (16.7%), ^{97}Mo (9.6%), ^{98}Mo (24.3%), ^{100}Mo (9.7%); ** lines with less than 10% intensities are not included; *** "tot"—the reaction produces the radionuclide directly and via decay of its metastable state.

2. Materials and Methods

2.1. Stacked-Foils Irradiations

Three experiments were performed at the ARRONAX facility [23], irradiating stacked-foils targets in vacuum with α beam of 67.4(5) MeV for about 1 h with beam currents of 40–60 nA. The stacked-foils technique and set-up in our facility have been described most recently in [24–26]. A typical stacked-foil target consisted of an Al monitor foil (~10 µm thick) in front, followed by the set of multiple ^{nat}Mo foils (~10 µm thick) and Al degraders (50–500 µm thick), arranged alternately. The order of the foils in the stacks were planned so that each ^{nat}Mo foil is activated with a different energy, all covering the energy range from 40 MeV to 67 MeV in about 3 MeV intervals (the projectile stopping-power in the stacks was calculated using SRIM software [27]). Certain foils were also used as catchers of the recoil atoms.

All foils were purchased from the GoodFellow© company with a purity of 99% for Al and 99.9% for ^{nat}Mo. Each foil was weighed before irradiation using an accurate scale (10^{-5} g) and scanned for area determination, allowing the precise thickness calculation (assuming the homogeneity over the whole surface).

As recommended by the International Atomic Energy Agency [28], the activity of the ^{24}Na radioisotope formed in Al monitor foil was used to calculate the beam current impinging the stack. Additionally, during the irradiations, the online beam current monitoring was performed using a Faraday's Cup with an electron suppressor for precise measurement and located behind the stack. The two measurements were consistent with each other.

2.2. Gamma Spectroscopy and Data Analysis

After about 14 h of cooling time, the gamma ray spectra of irradiated samples were collected using a HPGe Canberra detector with efficiency 20% at 1.33 MeV equipped with low-background lead and copper shielding. Each foil was placed at a height of 19 cm from the detector to ensure the dead-time below 10%. The detector was calibrated in energy and efficiency at 19 cm with [57]Co, ^{60}Co and [152]Eu calibrated sources from LEA-CERCA (France) prior to the measurements. Gamma spectra were recorded using the LVis software from Ortec© while the activity of the radionuclides produced at the End of Bombardment (EOB) were derived using the FitzPeaks Gamma Analysis and Calibration Software (JF Computing Services). For the identification and activity estimation we used the γ-line and associated branching presented in Table 1. Knowing the activity of each isotope and the thickness of the foil in which they were observed, it was possible to calculate their production cross-section σ with the following formula:

$$\sigma = \frac{A_{EOB}\, M\, Z\, e}{H\, N_A\, I\, \rho\, x\, (1 - exp\{-\lambda\, t\})}$$

where: A_{EOB}—activity of the radioisotope at the EOB, M—atomic mass of the target, Z—ionization number of the projectile, e—elementary charge, H—enrichment and purity of the foil, N_A—Avogadro's number, I—beam current, ρ—target material density, x—thickness of the foil, λ—decay constant of the radioisotope, t—time of the irradiation. The similar formula, solved for I and with cross-section values from [28], was used to calculate the beam current from the monitor foils. The projectile energy in the middle of the foils was adopted to the corresponding cross-section value.

The errors of cross-section values were propagated from the uncertainty of thickness measurements (around 1%), uncertainty of the counts in the γ-line peaks in the spectroscopy measurements (around 5–10%) and the error of the calculated beam current (around 5–10%) while the corresponding energy errors were propagated with SRIM software [27] considering the beam energy straggling through the foils (the initial energy error estimated by the cyclotron operators was 0.5 MeV).

The obtained cross-section values are then compared with TENDL-2017 (TALYS-based evaluated nuclear data library) [29] and the experimental results from other research groups.

2.3. Radionuclide Yield Calculator

Given the cross-section values, one can calculate the Thick Target Yield (TTY) with the following formula [30,31]:

$$TTY(E) = \frac{H\, N_A\, \lambda}{Z\, e\, M} \int_{E_{min}}^{E_{max}} \frac{\sigma(E)}{dE/dx(E)} dE$$

where: E_{max} and E_{min}—maximal and minimal energy of the projectile penetrating the target (in case of TTY, $E_{min} \leq$ reaction threshold), dE/dx—stopping-power of the projectile in the irradiated target. To facilitate this calculation for [97]Ru, as well as any other radioisotope and cross-section, we developed a Radionuclide Yield Calculator, later named RYC.

RYC is graphical user interface software written in python programming language (version 2.7) [32] using the TKinter module and compiled with PyInstaller software (version 3.4) [33]. It uses the cross-section and basic target data inputs to instantly calculate TTY and activity produced in any irradiation scenario. Data points can be fitted using different type of function, gaussian-like and polynomial functions, using the least-squares method. Excitation functions from TENDL [29] can be easily imported to compare with experimental data and to look for potential radioactive impurities. RYC with its detailed documentation can be downloaded from the ARRONAX website [34]. In particular, RYC uses implemented SRIM module [27] for stopping-power calculation.

The validation of this software was performed using data from the literature. On Figure 1, we compare the RYC-calculated TTY with the values published by IAEA [28,35] based on the same

cross-section values for ^{127}I(p,3n)^{125}Xe, ^{64}Ni(d,2n)^{64}Cu and ^{209}Bi(α,2n)^{211}At reactions on metallic targets. Data calculated by RYC are presented as points whereas the curve published by IAEA correspond to the lines. As can be seen, for the 3 types of projectiles and for the different target masses, a very good agreement is obtained. The same good results have been obtained for all our tests.
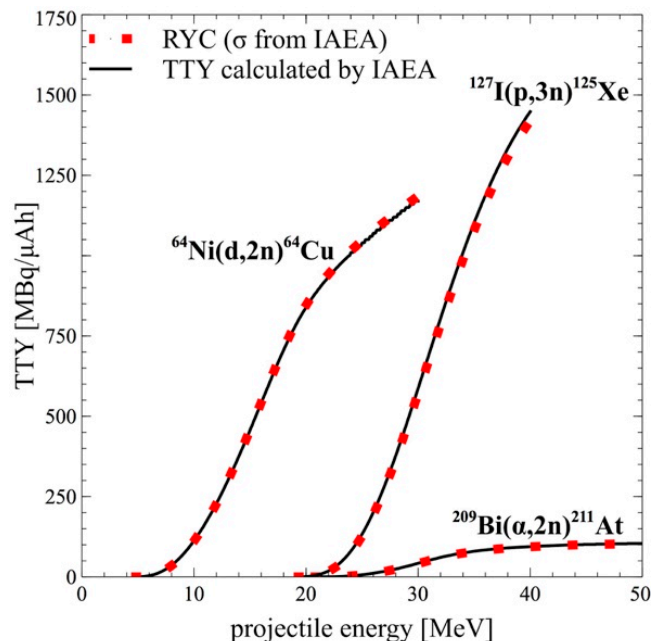

Figure 1. Comparison of TTY for selected nuclear reactions on metallic targets calculated with RYC and adapted from [28,35] based on the same cross-section values from IAEA.

3. Results and Discussion

3.1. Cross-Section Measurements

On Figures 2–6 we present the measured cross-sections for ^{nat}Mo(α,x) reactions producing the ^{97}Ru radioisotope as well as observed radioactive impurities: ^{89g}Zr, ^{95g}Tc, ^{96g}Tc, and ^{99}Mo. The contributing reactions forming these radioisotopes are shown in Table 1. The experimental data are compared with previous experiments reported in literature [3,19,20] and the values from TENDL-2017 library [29]. Measured cross-section values are also listed in Table 2 (with corresponding energy errors, not visible on the graphs).

Table 2. Measured cross-sections for ^{nat}Mo(α,x) reactions (with the uncertainties in the parenthesis).

E [MeV]	^{nat}Mo(α,x) Cross-Section [mb]				
	^{97}Ru	^{89g}Zr	^{95g}Tc	^{96tot}Tc	^{99}Mo
41.80(75)	237(20)	ND*	81(11)	73(7)	7.5(1.0)
46.03(68)	225(20)	ND	127(14)	89(8)	10.1(1.2)
50.00(64)	199(18)	ND	163(17)	100(9)	11.4(1.3)
51.93(62)	166(14)	ND	170(16)	101(9)	12.8(1.3)
55.30(60)	159(13)	3.6(9)	177(17)	109(9)	13.5(1.4)
58.51(56)	176(15)	11.7(1.6)	205(17)	119(10)	ND
59.97(55)	176(15)	18(2)	174(24)	116(10)	14.0(1.5)
63.47(53)	180(16)	30(3)	188(16)	118(10)	15.0(1.7)
66.84(50)	173(14)	40(3)	203(17)	122(10)	15.6(1.3)

* ND = not detected.

In the case of ^{97}Ru production (Figure 2), our measurements correspond well to the data at lower energies. Compared to the experimental data, TENDL shows similar structure but underestimates the cross-section by about 30 mb in the region 20–40 MeV. The subsequent fall of the excitation function and a bump seem to be shifted by 5–10 MeV with respect to the experimental data.
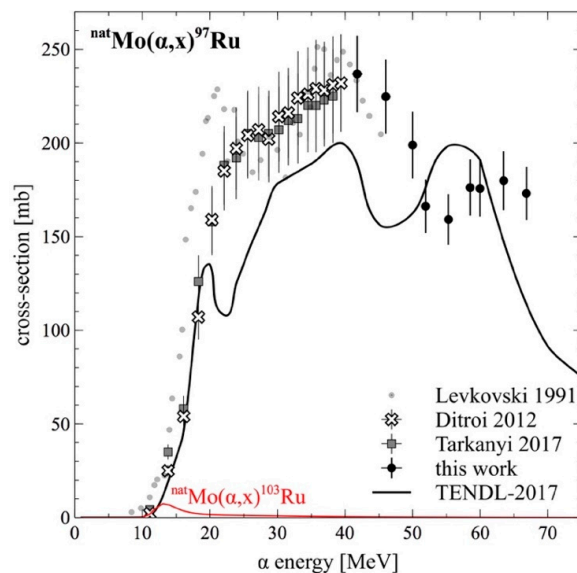

Figure 2. Measured cross-section for ^{nat}Mo(α,x)^{97}Ru reaction compared with data available in the literature. The coproduction of ^{103}Ru via ^{100}Mo(α,n)^{103}Ru and ^{100}Mo(α,p)^{103}Tc$\rightarrow$^{103}Ru reactions was not observed in the investigated energy range, but the cross-section for ^{nat}Mo(α,x)^{103}Ru from TENDL-2017 is plotted (red line) to complement the discussion from the text.

The ^{89g}Zr excitation function (Figure 3) is measured for the first time. The predictions of TENDL shows a similar trend as our measurements but with a slightly shifted toward lower energies (5 MeV).
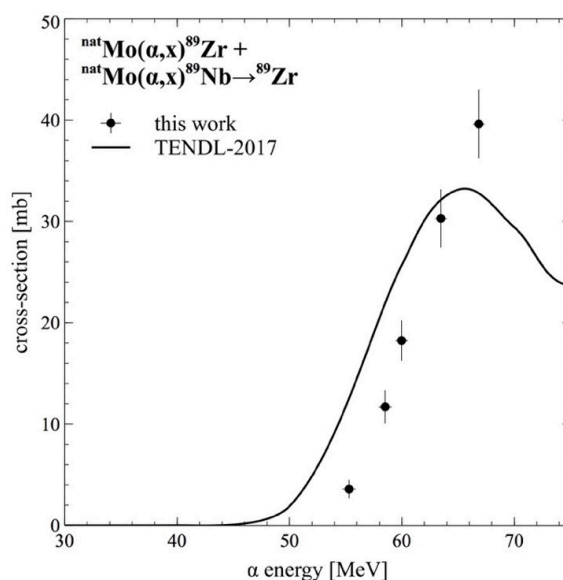
Figure 3. Measured cross-section for ^{nat}Mo(α,x)^{89g}Zr reaction compared with TENDL.

For ^{95g}Tc (Figure 4), our measurements are consistent with the previously measured data at lower energies. The shape of TENDL calculations seems to be the same as obtained in the measurements, but again a shift in energy is observed. This shift is probably related to the code since 3 different sets

of data acquired at different time, different laboratories and overlapping energy range are consistent with each other and shows the same shift with respect to TENDL.
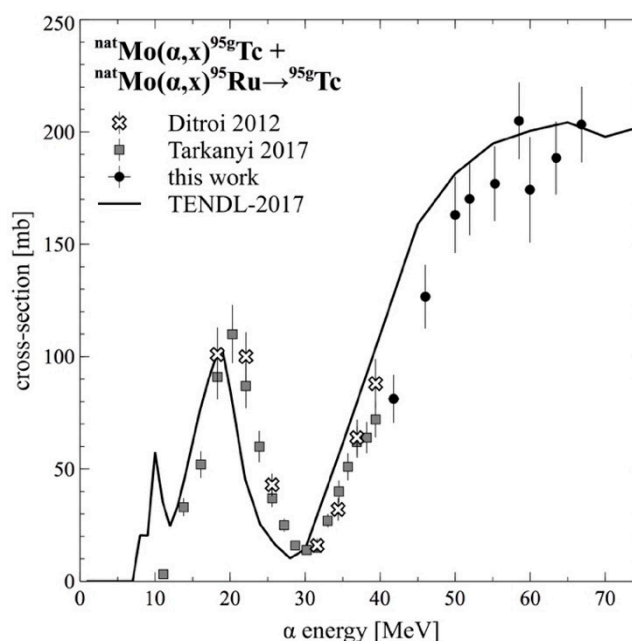

Figure 4. Measured cross-section for $^{nat}Mo(\alpha,x)^{95g}Tc$ reaction compared with the literature.

The experimental data describes well the excitation function for $^{96tot}Tc$ (Figure 5). Additionally, our measurements preserve the trend of the ones reported earlier for lower energies. Here we do not observe any shift with respect to the TENDL calculations, as seen in the previous reactions.
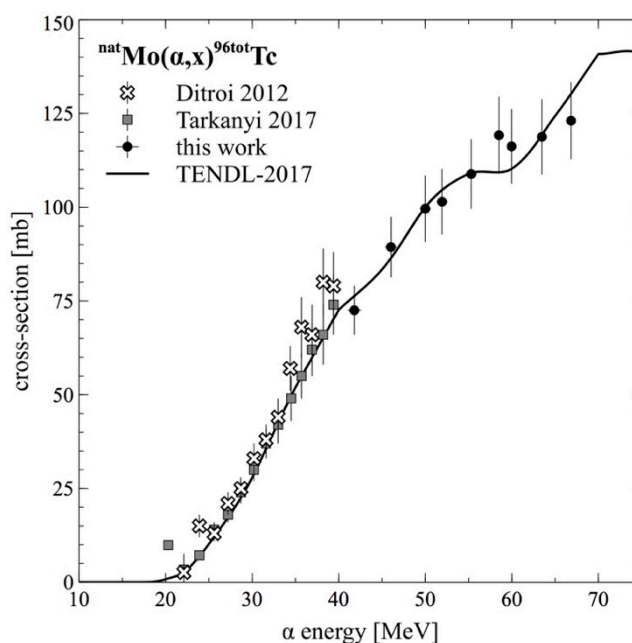
Figure 5. Measured cross-section for $^{nat}Mo(\alpha,x)^{96tot}Tc$ reaction compared with the literature. This is a cumulative cross-section of $^{nat}Mo(\alpha,x)^{96g}Tc$ and $^{nat}Mo(\alpha,x)^{96m}Tc$ reactions.

The experimental cross-sections for ^{99}Mo production (Figure 6) are consistent. Our results show a continuous rise of the excitation function up to the maximum energy of our measurements. This is in

obvious contrast to TENDL which predicts a maximum at around 30 MeV and then a decrease of the excitation function. Slight shift between TENDL and experimental results is observed at low energies.
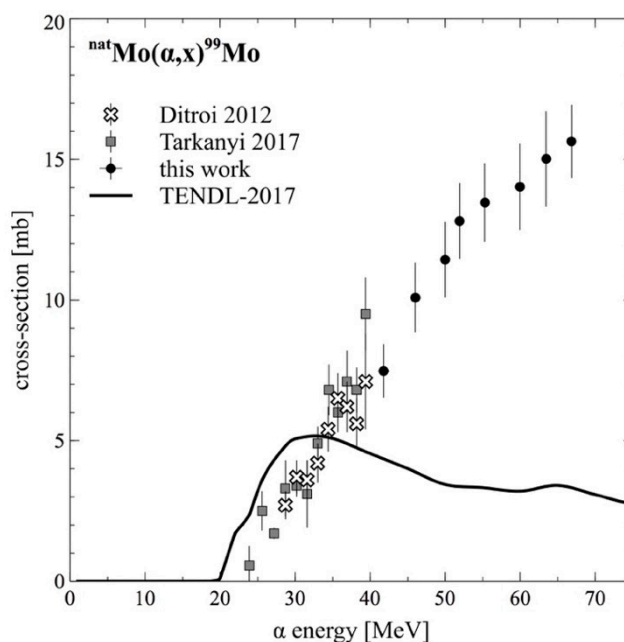

Figure 6. Measured cross-section for $^{nat}Mo(\alpha,x)^{99}Mo$ reaction compared with the literature.

3.2. Calculated Yield and Production

Using RYC, we calculated TTY for $^{nat}Mo(\alpha,x)^{97}Ru$ reaction on metallic ^{nat}Mo target, based on our cross-section measurements above 40 MeV and the values reported by [3,20] below 40 MeV (Figure 7). The TTY values for other radioisotopes were also calculated in a similar way (not shown) to estimate the radioactive impurities.
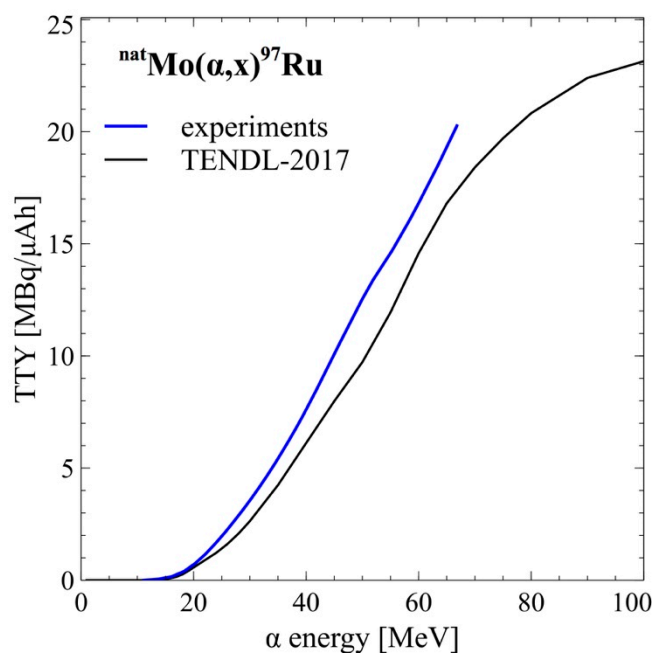

Figure 7. TTY for ^{97}Ru production via $^{nat}Mo(\alpha,x)$ on metallic ^{nat}Mo target. The experimental curve (blue) is calculated using the cross-section from this work (above 40 MeV) and the data provided by [3,20] below 40 MeV.

The obtained experimental TTY values for [97]Ru and radioactive impurities were used to estimate the possible production of [97]Ru (Table 3) with [nat]Mo target and for two energies: 30 MeV and 67 MeV, which are the most common in commercially available cyclotrons. The [97]Ru production yields are 3.5 MBq/μAh and 20 MBq/μAh respectively. Although the yield is almost 6 times larger at 67 MeV than at 30 MeV, the latter energy of α beam offer for example the optimal production of [211]At (summarized recently by [36]) and [43]Sc [37] medical radioisotopes. Additionally, in Table 3 we show the possible production of 50 MBq as this amount was proven SPECT-applicable in several clinical trials [38]. We have also calculated the yield and the number of produced stable Ru atoms ([96]Ru, [98]Ru, [99]Ru, [100]Ru, [101]Ru, [102]Ru) based on the TENDL cross-sections to estimate the specific activity (SA) of [97]Ru. The SA presented here assumes 100% successful chemical extraction of Ru isotopes from Mo target at EOB and hence is just an estimation used to compare different production routes.

It is worth mentioning that from the diagnostics point of view, the most dangerous impurity is [103]Ru. It is the only other radioactive Ru element with long half-life ($T_{1/2}$ = 39.26 d), which will contribute to the patient's dose via high-intensity gamma-line (497 keV with 90.9% intensity) and Auger electrons from its daughter ([103m]Rh). During the irradiation of [nat]Mo with α beam it can be only formed via [100]Mo(α,x) reactions marked as the red line on Figure 2. Its contribution is rather small in our energy range and its activity was below our detection limit but we address it nevertheless (based on the measurements of [3,20]).

For the completeness of this study, we show the alternative production of [97]Ru with the use of 100% enriched [95]Mo and [96]Mo targets and α beams of 30–15 MeV and 67–15 MeV, respectively.

Table 3. Estimation of [97]Ru activity produced via the irradiation of [nat]Mo (based on experimental data) and enriched [95,96]Mo targets (based on TENDL-2017 [29]) with α beam in two energy ranges. The list of radioactive impurities is narrowed down to the long-lived ones and shows their activity relative to activity of [97]Ru at EOB.

α energy		30–15 MeV		67–15 MeV	
target		[nat]Mo	[95]Mo (100%)	[nat]Mo	[96]Mo (100%)
thickness		100 mg/cm^2	100 mg/cm^2	540 mg/cm^2	540 mg/cm^2
[97]Ru yield		3.5 MBq/μAh	14 MBq/μAh	20 MBq/μAh	31 MBq/μAh
irradiation		1 h, 15 μA	1 h, 15 μA	1 h, 2.5 μA	1 h, 2.5 μA
[97]Ru A$_{EOB}$		50 MBq (1.4 mCi)	200 MBq (5.4 mCi)	50 MBq (1.4 mCi)	80 MBq (2.2 mCi)
SA at EOB		350 GBq/μmol (9 kCi/mmol)	1300 GBq/μmol (36 kCi/mmol)	420 GBq/μmol (11 kCi/mmol)	630 GBq/μmol (17 kCi/mmol)
relative activity [%]	**[97]Ru**	100	100	100	100
	[89g]Zr	0	0	3	0.04
	[95g]Tc	95	1E−3	200	150
	[96g]Tc	4	0.2	25	34
	[103]Ru	0.12	0	0.02	0
reference		[3], [20]	TENDL-2017	[3], [20] this work	TENDL-2017

Further chemical separation would be required to extract Ru element from Mo target and separate it from formed radioactive and stable elements of Tc, Nb, and Zr. This can be done for example with either the solvent extraction or distillation methods with an efficacy better than 80% [16]. The SA should also be considered in further chemical research as each production route form additional stable atoms of Ru, which would chelate the labeling compound.

4. Conclusions and Summary

We have extended the available cross-section measurements of selected ^{nat}Mo(α,x) reactions up to 67 MeV. Our measurements preserve well the trend of the cross-section values reported previously below 40 MeV and are consistent in overlapping energy ranges. A reasonable agreement with TENDL is observed however in certain cases the shift of 5–10 MeV is visible with respect to the experimental data.

We have shown the feasibility of no-carrier-added ^{97}Ru production with α beam up to 67 MeV and thick ^{nat}Mo targets. The impurity of the only long-lived radioactive Ru radioisotope (^{103}Ru) is small, around 0.1%. An irradiation of 1 h with few μA α-beam should satisfy the need for SPECT imaging for the patient. Several doses could be produced with longer irradiations at higher currents or using enriched ^{95,96}Mo targets which will substantially increase the produced activity and SA.

The use of RYC [34] to calculate TTY based on cross-section data was also demonstrated.

Conflicts of Interest: The authors declare no conflict of interest.

References

1. Subramanian, G.; McAfee, J.G.; Poggenburg, J.K. Ruthenium-97: A preliminary evaluation of a new radionuclide for use in nuclear medicine. *J. Nucl. Med.* **1970**, *11*, 365.
2. Maiti, M.; Lahiri, S. Measurement of yield of residues produced in ^{12}C+^{nat}Y reaction and subsequent separation of ^{97}Ru from Y target using cation exchange resin. *Radiochim. Acta* **2015**, *103*, 7–13. [CrossRef]
3. Tárkányi, F.; Hermanne, A.; Ditrói, F.; Takács, S.; Ignatyuk, A. Investigation of activation cross section data of alpha particle induced nuclear reaction on molybdenum up to 40 MeV: Review of production routes of medically relevant ^{97,103}Ru. *Nucl. Inst. Meth. B* **2017**, *399*, 83–100. [CrossRef]
4. Zaitseva, N.G.; Stegailov, V.I.; Khalkin, V.A.; Shakun, N.G.; Shishlyannikow, P.T.; Bukow, K.G. Metal Technetium Target and Target Chemistry for the Production of ^{97}Ru via the ^{99}Tc(p,3n)^{97}Ru Reaction. *Appl. Radiat. Isot.* **1996**, *47*, 145–151. [CrossRef]
5. Mukhopadhyay, B.; Mukhopadhyay, K. Applications of the Carrier Free Radioisotopes of Second Transition Series Elements in the Field of Nuclear Medicine. *J. Nucl. Med. Radiat. Ther.* **2011**, *2*, 1000115. [CrossRef]
6. Shao, H.S.; Meinken, G.E.; Srivastava, S.C.; Slosman, D.; Sacker, D.F.; Sore, P.; Brill, A.B. In vitro and in vivo characterization of ruthenium bleomycin compared to cobalt- and copper-bleomycin. *J. Nucl. Med.* **1986**, *27*, 1044.
7. Clarke, M.J. Ruthenium in Cancer Chemotherapy. *Platin. Met. Rev.* **1988**, *32*, 198.
8. Ku, T.H.; Richards, P.; Srivastava, S.C.; Prach, T.; Stang, L.G., Jr. Production of ruthenium-97 for medical applications. In Proceedings of the 2nd International Congress of the World Federation of Nuclear Medicine and Biology, Washington, DC, USA, 17–21 September 1978.
9. Lagunas-Solar, M.C.; Avila, M.J.; Navarro, N.L.; Johnson, P.C. Cyclotron Production of No-carrier-added ^{97}Ru by Proton Bombardment of ^{103}Rh Targets. *J. Appl. Radiat. Isot.* **1983**, *34*, 915–922. [CrossRef]
10. Lebowitz, E.; Kinsley, M.; Klotz, P.; Bachsmith, C.; Ansari, A.; Richards, P.; Atkins, H.L. Development of ^{97}Ru and ^{67}Cu for medical use. *J. Nucl. Med.* **1974**, *15*, 511.
11. Zaitseva, N.G.; Rurarz, E.; Vobecký, M.; Hwan, K.H.; Nowak, K.; Téthal, T.; Khalkin, V.A.; Popinenkova, L.M. Excitation function and yield for ^{97}Ru production in ^{99}Tc(p,3n)^{97}Ru reaction in 20–100 MeV proton energy range. *Radiochim. Acta* **1992**, *56*, 59–68. [CrossRef]

12. Dmitriev, S.N.; Zaitseva, N.G.; Starodub, G.Y.; Maslov, O.D.; Shishkin, S.V.; Shishkina, T.V. High-purity radionuclide production: Material, construction, target chemistry for ^{26}Al, ^{97}Ru, ^{178}W, ^{235}Np, ^{236,237}P. *Nucl. Inst. Meth. A* **1997**, *397*, 125–130. [CrossRef]

13. Uddin, M.S.; Hagiwara, M.; Baba, M.; Tarkanyi, F. Experimental studies on excitation functions of the proton-induced activation reactions on silver. *Appl. Radiat. Isot.* **2005**, *62*, 533–540. [CrossRef] [PubMed]

14. Ditrói, F.; Tárkányi, F.; Takács, S.; Mahunka, I.; Csikai, J.; Hermanne, A.; Uddin, M.S.; Hagiwara, M.; Baba, M.; Ido, T.; et al. Measurement of activation cross sections of the proton induced nuclear reactions on palladium. *J. Radioanal. Nucl. Chem.* **2007**, *272*, 231–235. [CrossRef]

15. Mito, A.; Komura, K.; Mitsugashira, T.; Otozai, K. Excitation functions for the (d, p) reactions on ^{96}Ru, ^{102}Ru and ^{104}Ru. *Nucl. Phys. A* **1969**, *129*, 165–171. [CrossRef]

16. Comparetto, G.; Qaim, S. A Comparative Study of the Production of Short-Lived Neutron Deficient Isotopes ^{94,95,97}Ru in α- and ^{3}He-Particle Induced Nuclear Reactions on Natural Molybdenum. *Radiochim. Acta* **1980**, *27*, 177–180. [CrossRef]

17. Maiti, M.; Lahiri, S. Production and separation of ^{97}Ru from ^{7}Li activated natural niobium. *Radiochim. Acta* **2011**, *99*, 359–364. [CrossRef]

18. Maiti, M. Production and separation of ^{97}Ru and coproduced ^{95}Tc from ^{12}C-induced reaction on yttrium target. *Radiochim. Acta* **2013**, *101*, 437–444. [CrossRef]

19. Levkovski, V.N. *Cross-Section of Medium Mass Nuclide Activation (A = 40–100) by Medium Energy Protons and Alpha-Particles (E = 10–50 MeV)*; Inter-Vesi: Moscow, Russia, 1991.

20. Ditrói, F.; Hermanne, A.; Tárkányi, F.; Takács, S.; Ignatyuk, A.V. Investigation of the α-particle induced nuclear reactions on natural molybdenum. *Nucl. Inst. Meth. B* **2012**, *285*, 125–141. [CrossRef]

21. Poirier, F.; Girault, F.; Auduc, S.; Huet, C.; Mace, E.; Delvaux, J.I.; Haddad, F. The C70 Arronax and beam lines status. In Proceedings of the IPAC2011, San Sebastián, Spain, 4–9 September 2011.

22. International Atomic Energy Agency, Live Chart of Nuclides. 2018. Available online: https://www-nds.iaea.org/relnsd/vcharthtml/VChartHTML.html (accessed on 21 January 2019).

23. Haddad, F.; Ferrer, L.; Guertin, A.; Carlier, T.; Michel, N.; Barbet, J.; Chatal, J.F. ARRONAX, a high-energy and high-intensity cyclotron for nuclear medicine. *Eur. J. Nucl. Med. Mol. Imaging* **2008**, *35*, 1377–1387. [CrossRef] [PubMed]

24. Garrido, E.; Duchemin, C.; Guertin, A.; Haddad, F.; Michel, N.; Métivier, V. New excitation functions for proton induced reactions on natural titanium, nickel and copper up to 70 MeV. *Nucl. Inst. Meth. B* **2016**, *383*, 191–212. [CrossRef]

25. Guertin, A.; Duchemin, C.; Fardin, A.; Guigot, C.; Nigron, E.; Remy, C.; Haddad, F.; Michel, N.; Métivier, V. How nuclear data collected for medical radionuclides production could constrain nuclear codes. In *EPJ Web of Conferences*; EDP Sciences: Les Ulis, France, 2017; p. 146.

26. Pupillo, G.; Sounalet, T.; Michel, N.; Mou, L.; Esposito, J.; Haddad, F. New production cross sections for the theranostic radionuclide ^{67}Cu. *Nucl. Inst. Meth. B* **2018**, *415*, 41–47. [CrossRef]

27. Ziegler, J.F.; Ziegler, M.D.; Biersack, J.P. SRIM Code, Version 2008.04. Available online: http://www.srim.org/ (accessed on 21 January 2019).

28. International Atomic Energy Agency. Charged-Particle cross Section Database for Medical Radioisotope Production: Diagnostic Radioisotopes and Monitor Reactions. 2017. Available online: https://www-nds.iaea.org/medical (accessed on 21 January 2019).

29. Koning, A.J.; Rochman, D. Modern Nuclear Data Evaluation with The TALYS Code System. *Nucl. Data Sheets* **2012**, *113*, 2841–2934. [CrossRef]

30. Phelps, M.E. *PET: Molecular Imaging and Its Biological Applications*; Springer: New York, NY, USA, 2004.

31. de Lima, J.J.P. *Nuclear Medicine Physics*; CRC Press: Boca Raton, FL, USA, 2011.

32. Python Software Foundation. Python Programming Language, Version 2.7. 2010. Available online: https://www.python.org (accessed on 21 January 2019).

33. Cortesi, D. PyInstaller Documentation, Release 3.4. 2018. Available online: https://www.pyinstaller.org/documentation.html (accessed on 21 January 2019).

34. ARRONAX, Radionuclide Yield Calculator. 2018. Available online: http://www.cyclotron-nantes.fr/spip.php?article373 (accessed on 21 January 2019).

35. International Atomic Energy Agency. Cross Section Database for Medical Radioisotope Production: Production of Therapeutic Radionuclides. 2011. Available online: https://www-nds.iaea.org/radionuclides (accessed on 21 January 2019).

36. Kim, G.; Chun, K.; Park, S.H.; Kim, B. Production of α-particle emitting [211]At using 45 MeV α-beam. *Phys. Med. Biol.* **2014**, *59*, 2849. [CrossRef] [PubMed]

37. Szkliniarz, K.; Sitarz, M.; Walczak, R.; Jastrzębski, J.; Bilewicz, A.; Choiński, J.; Jakubowski, A.; Majkowska, A.; Stolarz, A.; Trzcińska, A.; et al. Production of medical Sc radioisotopes with an alpha particle beam. *Appl. Radiat. Isot.* **2016**, *118*, 182–189. [CrossRef]

38. Zanzi, I.; Srivastava, S.C.; Meinken, G.E.; Robeson, W.; Mausner, L.F.; Fairchild, R.G.; Margouleff, D. A New Cholescintigraphic Agent: Ruthenium-97-DISIDA. *Nucl. Med. Biol.* **1989**, *16*, 397–403. [CrossRef]